Engineering Science and Military Technologies
Volume (4) - Issue (1) - Mar 2020

ISSN: 2357- 0954
DOI: 10.21608/ejmtc.2020.27784.1141

Integrating CAM and numerical simulation to investigate single point incremental forming of Al6061

Original Article

Amr Shaaban, Ahmed Samy Elakkad

Department of Designs and Production, Faculty of Engineering, Ain Shams University, Cairo, Egypt

Keywords:
CAM, CNC, metal forming simulation, SPIF.

Corresponding Author:
Ahmed Samy Elakkad, Department of Designs and Production, Faculty of Engineering, Ain Shams University, Cairo, Egypt, **Tel:** +201000735559, **Email:** ahmed.elakkad@eng.asu.edu.eg

Abstract
Single point incremental forming, SPIF, is a forming process that has a great potential application in sheet metal industries. SPIF is capable of producing medium size batches of complex shapes with low cost as it requires no die. This study explores the potentials of integrating computer aided manufacturing, CAM, and finite element analysis, FEA, to obtain a virtual model that realistically simulates the SPIF process. The simulation of SPIF process has been carried out using LS-Dyna4.3© software while producing a circular and rectangular taper pockets on a blank made of AL6061. The tool path has been generated using a CAM software and imported to a CNC machine to execute the SPIF process, taking into consideration the main forming parameters: the feed rate and the incremental step size. The results of both simulation and experiment are presented against each other in terms of thickness reduction, springback, and cross-sectional profile, and they are proved to be close within an accepted range. The virtual model obtained in this study is believed to be useful for performing an optimization analysis to decide the optimum forming parameters that are thought to affect the SPIF process.

I. INTRODUCTION

Over the past decade, Single Point Incremental Forming, SPIF, has interested researchers as a forming process that requires no dedicated die, and hence saves time and effort. Unlike conventional forming processes, SPIF relies instead on employing CAM/CNC to generate a tool path, but one that is assigned to a forming tool rather than the endmill usually used for milling[1]. The process simply consists of a blank, which is fixed to the machine table using a special attachment; a tool, which forms the blank continuously following a predefined path; and a vertical milling CNC machine. The SPIF is similar to a spinning process and it is often said that SPIF has evolved from it[2]. In addition, SPIF is considered a type of incremental sheet forming, ISF, and is also called the negative incremental forming, NIF, whereas there is another type of ISF known as two Point Incremental Forming, TPIF, or also called the positive incremental forming. The main difference between both types is that SPIF is completely die-less forming, while the TPIF uses a partial die[3]. One of the main advantages of SPIF is its relatively high forming limit. The forming limit is defined as the maximum deformation achieved before reaching failure. Many researches have proved that the strains incurred by the material in the SPIF process are much higher than other forming processes [4]. Other studies have been concerned with the study of the parameters that may affect the formability in NIF. Hussein *et al.*[5] have introduced a comprehensive study on the effect of the thinning band on the formability of NIF. They define the thinning band as a severe decrease in the thickness that occurs when the wall angles approach the maximum attainable[5].

They employ the VWACF test which has been previously created by the same authors[6]. The test has been performed on four materials. They have eventually found that the formability is not affected by the thinning band unless it occurs in the flange area, and that the fracture in most cases occurs naturally when the material reaches the normal formability limit[5]. Another attempt to improve the formability was made by Naranjo *et al.*[7]. They have worked on Ti6Al4V which is known by its low formability. They prove that using SPIF at high temperature (300-400 ºC) can help to attain better forming characteristics, reduce forces, and substantially reduce springback.

It has also been proved that SPIF can be applicable for wide range of materials in industry such as steel, titanium, brass, and aluminium alloys[8]. SPIF also has contributions in various fields of industry such as aerospace, automotive, and even biomedical. For example, Eksteen and Van der Merwe[9] introduce a study through which they employ

the characteristics of titanium to produce plate implants for minimalinvasive surgical procedures[9]. In addition, valuable efforts have been done by Popp, Rusu, Racz, and Popp[10] to producecranial implants using the SPIF. They use finite element analysis, FEA, to predict the thickness and forces exerted while manufacturing the implants using SPIF[10].

Many parameters are included while designing the SPIF process. The two basic parameters of the most influence are the feed rate (f_r mm/min) and the incremental step size in Z direction (δzmm/path), while path is defined as one complete revolution of the tool around the axes of the centre of the blank. Nevertheless, there are other parameters that also have significant impact on SPIF such as the material, the thickness of the blank, the tool diameter, the degree of complexity of the desired feature, the forming angle (α), and tool path strategy[11]. On the other hand, in order to evaluate this process, the process responses that should be addressed should at least include: the loads generated throughout the time of the forming process, the cross-sectional profile, and the thinning percentage (δt). Moreover, an essential limitation should be considered while designing those parameters that is avoiding high shear stresses that may lead to tearing the blank instead of stretching it. In this context, Al-Obaidi and Hamdan[12] present an experimental assessment of the factors affecting the SPIF. They set the surface roughness and thinning as the process responses and study experimentally how much they are affected by the change of incremental depth, feed rate, and spindle speed. They have found that the surface roughness is highly affected by the incremental depth in the first place, followed by the feed rate, while the thinning is proved to be mainly dependent on the spindle speed[12].

This multiplicity of theparameters affecting the SPIF process render it difficult to depend on the experimental method to introduce an informative study for the effect of each parameter, let alone performing an optimization analysis[13]. Therefore, attention has been directed towards exploring the potentials of numerical simulation. This study employs FEA to reach a simulation that can capture the physics of the SPIF process in real life. Yet, it requires a validation for the simulation, which is realized by carrying out an experiment of SPIF and comparing the results of both, the simulation and the experiment.

It is worthy to highlight the rise of a new technique recently used for the ISF which is ultrasonic vibration assisted, UVA. It is based on a fact that the material behavior quite differs under the effect of ultrasonic vibration, as the large vibration amplitude results in a large reduction in the flow stress, making the material softer to be formed[14].

In this study, the SPIF is employed to produce a circular and a rectangular taper pockets with the dimensions shown in Figure 1(a and b).

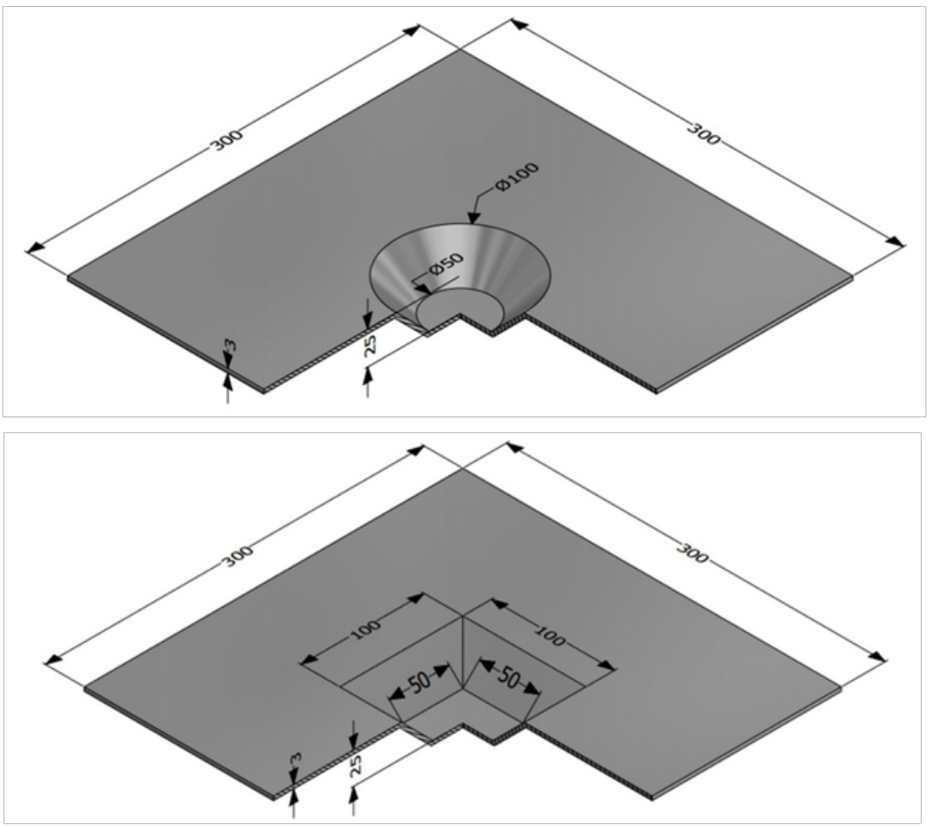

Fig. 1: The 3D model of the (a) circular and (b) rectangular pockets that is required to be formed using SPIF.

The blank upon which the SPIF process is carried out is fabricated from Al6061 alloy and its dimensions are defined as 300×300×3 mm. The dimensions of the circular taper pocket required to be formed is 100 mm, and 50 mm for the upper and lower diameters respectively. While the size of the upper and lower rectangles is 100×100 mm, and 50×50 mm for the rectangular taper pocket. Consequently, the forming angle α, which is the inclination angle of the deformed sheet, is 45º for both cases. Besides, the tool consists of a rod of a hemisphere shaped end of 10 mm diameter, manufactured out of steel K110, coated with nickel chrome. This study is carried out in the following steps: 1. The material is modelled through the finite element, FE, solver to guarantee the identicality of the material behavior in the numerical analysis to the material behavior in real life, 2. The tool paths that correspond to the circular and rectangular pocketsaregenerated, 3. The SPIF process is carried out experimentally and the predefined process responses are measured, 4. The forming process is analyzed, and the results are examined, and 5. The experimental results are compared to those obtained from thenumerical analysis to validate the numerical model. Thus, this study aims at investigating the validity and effectiveness of replacing experimental SPIF with a numerical model to facilitate the study of the process and to pave the way to more dedicated studies. The SPIF process is still relatively unfamiliar to the manufacturers in Egypt, because it is rather unusual to carry out a forming process without a die. It is hoped that this study will motivate the spread of this process in the future.

II. MODELLING OF MATERIAL CHARACTERISTICS OF AL6061

Material modelling is considered a primary and fundamental stage in any numerical analysis, for a realistic simulation can only be achieved when material properties have been correctly defined for the FE solver. To feed the FE solver with the material data required for the numerical simulation, these data need to be first obtained through an experimental tensile test. In this study, an experimental tensile test has been conducted on a standard specimen out of an AL6061 alloy; the same alloy upon which the SPIF experimentiscarried out. The data obtained from the experimentaltensile test provide the information that concern elasticity, represented in Young's Modulus E and Poisson's Ratiou, in addition to the yield, ultimate, and fracture stresses. The data also provide the necessary information required for defining plasticity properties, namely the stress-strain curve, starting from the yield point until the ultimate, known as the multilinear isotropic hardening curve. The obtained data concerning the plasticity properties, however, require modifications to be compatible with the FE solver.

II.1. TRUE STRESS-STRAIN CURVE

First, since the FE solver only accepts true values, and the stress-strain curve values obtained from the experimental tensile test are typically engineering, they must be initially converted into true values[15]. It should be kept in consideration that the validity of the conversion from engineering to true ends by the ultimate point, and that the true values beyond the ultimate (the necking) must be obtained by measuring the change in the area until the fracture point is reached. Fortunately, the material data needed for the simulation do not necessarily include defining the part of the stress-strain curve beyond the ultimate point, since the simulation of a metal forming process is naturally restricted by the ultimate point after which the process fails. Second, since the FE solver does not accept total strain values, the total strain values obtained from the experimental tensile test must be converted into equivalent plastic strain,EPS,values. These are determined by subtracting a variable valuefrom the total strain. This variable value is the ratio of the corresponding stress σ to the Young's modulus E.

II.2. NUMERICAL AND EXPERIMENTAL TENSILE TEST

The FE solver offers various models to define the plasticity zone. In this study, it has been assumed that the loading is not cyclic, which allows for neglecting the Bauschinger effect. Hence the isotropic hardening model has been selected rather than the kinematic hardening model. Thus, the material AL6061 has been defined to the FE solver and is registered in its library. In order to verify that the material modelling has been properly achieved, a simulation of the tensile test has been carried out and its results have been compared to those results obtained from the experimental tensile test. To carry out the simulation of the tensile test, the explicit analysis module available in Ansys18.0© has been employed.

According to the nature of the tensile test, the stress acting upon each element is uniaxial and in-plane. Accordingly, the strain in the load direction together with the lateral strain should be considered, while the stress variation through the thickness can be neglected. Therefore, using 2D elements is quite enough to model the specimen, rather than using 3D elements, which increases the size of the FE-model without a considerable gain. Eventually, a 2D surface model of the specimen following the standard dimensions is created and the FE model is built using quadrilateral shell elements. Then, a tensile load is set on both ends, so that it would be enough to exceed the ultimate stress. In order to simulate the fracture phase, the failure criterion has been set so that the elements would erode once their EPS reaches a value that is equivalent to the value corresponding to the ultimate stress. Since, as previously mentioned, the FE solvers only work with true stress and true strain values and can only

present the strain values as EPS, the stress strain values obtained from the simulation should first be modified so that they could be compared to those of the experiment. Thus, as shown in Figure 2, it can be proved that modelling the properties of AL6061 alloy has been achieved successfully.

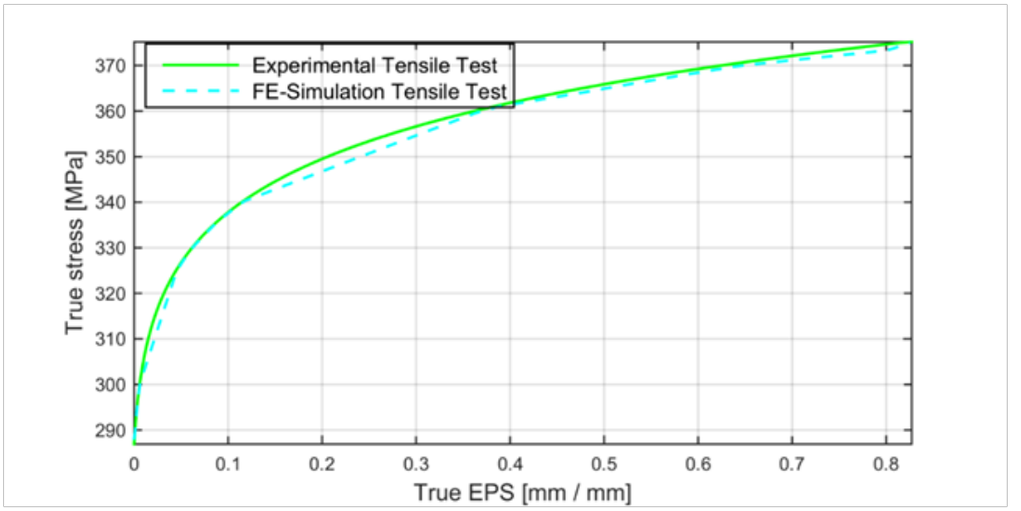

Fig. 2: The true EPS values versus the true stress values generated from experimental tensile test and from the numerical simulation.

III. TOOL PATH GENERATION

III.1. DESIGN OF THE TOOL PATH

One of the essential process parameters that should be clearly defined in a SPIF is the tool path of the tool. The tool path should be designed according to the desired shapes that need to be formed on the blank, which in this study are the circular and rectangular taper pockets. To generate the tool path, a CAM software has been employed prior to the simulation of the SPIF. Moreover, this tool path is required to carry out the SPIF experiment later. While a CAM software is generally used for machining rather than metal forming, it can be employed in this experiment to create the tool path required for the pockets as if it were a machining operation on a milling machine. It is worthy to highlight some valuable researches that have been conducted to optimize the tool path as that one introduced by Azaouzi and Lebaal[16]. They use the response surface method, RSM, to obtain an optimum tool path that reduces the manufacturing time, and simultaneously, homogenizes the thickness distribution. In the same context, Suresh, Khan, and Regalla[11] have introduced a methodology to generate the tool path defined with a specific strategy that suits the required feature; however, generating the tool path using a CAM software is found to be quite sufficient for the purpose of this study. Autodesk PowerMill 2019©, which is a CAM software package specialized for milling operations, has been employed to generate the numerical control, NC, file, which contains the part program. This file is used to extract the tool path information needed for the numerical simulation, and to execute the part program on the CNC milling machine as well. For that purpose, first, 3D models of the circular and rectangular taper pockets have been created, with the program zero initially set to be in the centre of the blank.

III.2. PARAMETERS AFFECTING THE TOOL PATH

The main parameter that affects the tool path, apart from the shape of the feature itself, is the δ_z (mm/path). The smaller this value is, the longer the tool path will be, and consequently, the greater the time required to finish the forming will be. Yet, the time required for the forming does not only depend on the δ_z, but also on the f_r (mm/min) by which the tool moves during the forming process. The tool diameter offset is considered while generating the path or otherwise the dimensions of the pocket would be larger than the desired value. Accordingly, the tool radius (5 mm) is subtracted from the X and Y coordinates of the path. In this study, for the circular pocket, the value of δ_z has been set to be 0.5 mm/path, while f_r is set as 4000 mm/min. This results in a length of 10.2 m for the tool path, and a time of 153 sec required for the forming process. Similarly, for the rectangular pocket, the value of δ_z has been set to be 0.2 mm/path, while f_r is 6000 mm/min. This results in a length of 65.28 m for the tool path, and a time of 653 sec required for the forming process. The reason behind selecting different values for the δ_z and f_r in both experiments is to allow for better understanding of its effect on the forming process. The tool paths for both the circular and rectangular taper pockets are shown in Figure 3 (a and b).

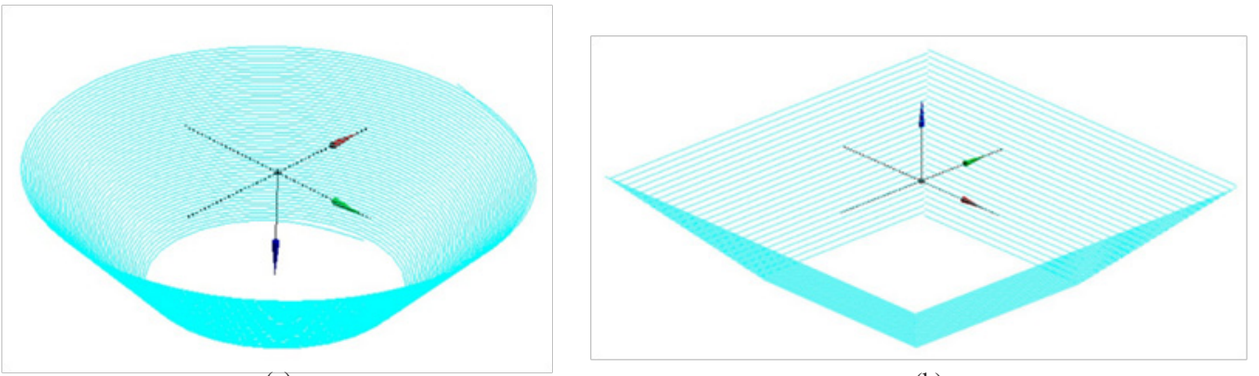

(a) (b)

Fig. 3: The tool path as generated by the CAM software for both (a) circular and (b) rectangular taper pockets.

IV. EXPERIMENTAL PROCEDURE

IV.1. EXPERIMENT SETUP

To carry out the SPIF process experimentally, the following is needed: CNC milling machine, fixation attachment, a blank, and a tool. A 4-axis CNC milling machine with a FANUC© controller (vertical machining center (VM702H)) has been selected; and a tool of 10 mm diameter has been manufactured out of steel K110, coated with nickel chrome to add to the hardness of the outer surface of the tool, to be able to resist the friction for a longer time. Figure 4 shows the tool mounted to the tool holder, while Figure 5 shows the attachment which consists of an upper and a lower frame, together with 4 bolts to fix the blank. The bolts have been tightened so as not to allow the blank to slip between the upper and lower frames while the experiment is in progress.

Fig. 4: A tool of 10 mm diameter with rounded head and manufactured of K110 coated with nickel chrome.

The width of the strip of the blank under clamping should be set within 10% to 20% of the overall blank width so that a sufficient space for the forming process is allowed, or else it would lead to high stresses on the blank that may result in shearing instead of forming

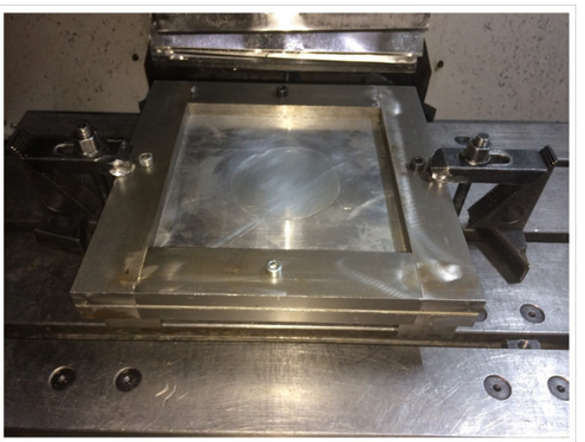

Fig. 5: The fixing attachment for the blank clamped to the CNC machine table.

However, a deviation is expected in the resulting profile compared to the desired one, due to the relatively larger free zone in the centre of the blank. This is known as blank bending. The clamping width has been chosen as 40 mm for both experiments of circular and rectangular taper pockets. Another deviation is expected in the centre of the blank called the pillow effect, which results from

the fact that this area is not exposed to the direct stresses imposed by the tool throughout the forming process. The whole attachment is then mounted on the machine table using clamps, and the program zero is manually set at the centre upper face of the blank. Finally, the NC code generated by the CAM software is imported to the CNC machine. The experiment has thus been carried out for the circular and rectangular taper pockets, resulting in the forms shown in Figure 6 (a and b).

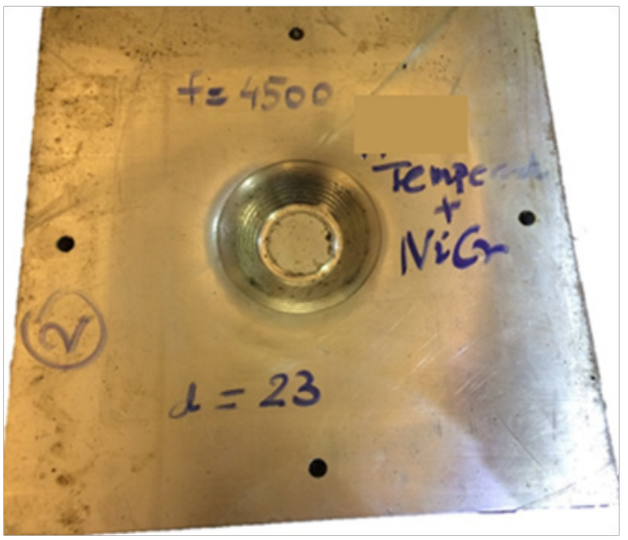

(a)

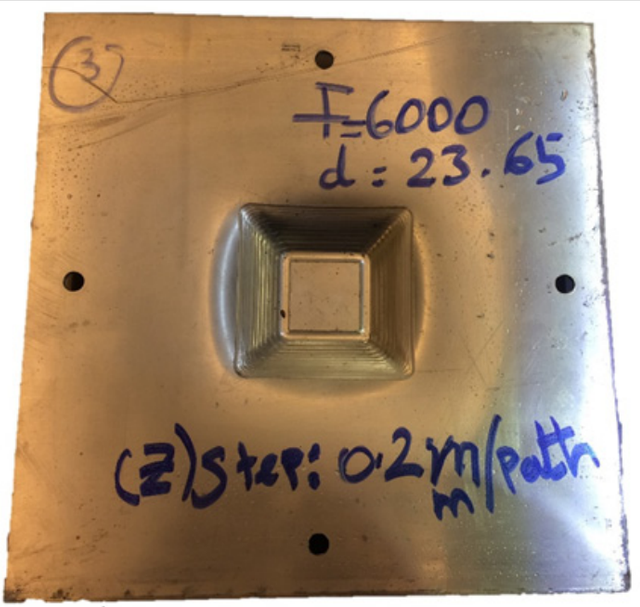

(b)

Fig. 6: The final product after SPIF process has been carried out experimentally for (a) circular and (b) rectangular taper pockets.

IV.2. MEASURING THE CROSS-SECTIONAL PROFILE

After the forming process is over, a method had to be devised to measure the profile. The deformed blank has been cut into two halves using a saw on a conventional milling machine. The cutting conditions and fixation method have been selected carefully, so that no high forces are produced, which could lead to a change in the profile form before measuring it. Tool room microscope has been used to find the profile in terms of XY coordinate points, as shown in Figure 7.

Fig. 7: Tool room microscope used to measure the cross-sectional profile of the manufactured pockets.

V. NUMERICAL SIMULATION OF SPIF USING LS-DYNA©

V.1. DEFINING THE SIMULATION APPROACH

Since SPIF is categorized as a metal forming process, the explicit dynamics analysis is logically selected for its capability of dealing with such non-linear and complicated material behaviour. In order to control the process parameters, basic information should be attained such as stress tensors, strain tensors, internal energy and forces. Since capturing the history of all previously mentioned parameters throughout the forming process is so difficult experimentally, numerical simulation is essentially needed [17]. This study uses LS-Dyna4.3© to carry out the numerical simulation of the SPIF process. LS-Dyna is a general-purpose FE solver that is widely used in the field of FEA specially in the field of metal forming simulation and vehicle design studies.

As previously mentioned, the SPIF process basically involves two parts: the blank and the tool. The purpose of performing any numerical simulation is to obtain a numerical model that can realistically simulate what happens in real life experiment. Therefore, the blank and the tool should both be carefully modelled considering many aspects for the FE-solver such as, geometry, material, meshing, and contacts.

V.2. MESH SETTINGS

The mesh quality is one of the factors that significantly affect the accuracy of any numerical simulation process, especially that the simulation of SPIF requires the use of explicit dynamic analysis, which is basically very sensitive for the mesh quality. What makes it that sensitive is that the value of the time step selected through the solving iterations is defined based on the element of the least quality. The presence of only one distorted element in the FE model can lead to an undesired small-time step, and consequently result in an unacceptably large solving time.

Therefore, the mesh of the blank has been designed to be divided into two regions: the region at the edges at which the blank is clamped, and the region at the centre where the forming process is to be carried out. The size of the mesh and the division of regions have been adjusted so that the region at the centre has a finer mesh while maintaining a proper aspect ratio for each element and a smooth transition of element size between the two regions. The design of the mesh for both blank and tool is shown in Figure 8.

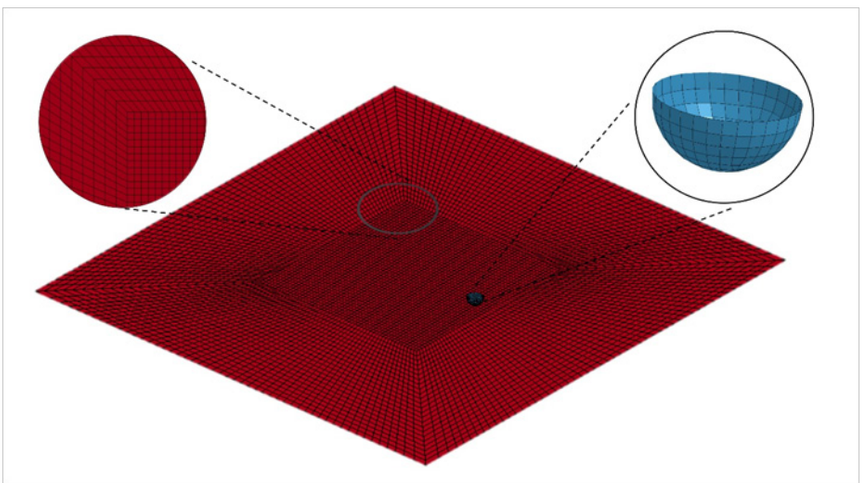

Fig. 8: The design of the mesh for the blank and the tool.

Shell elements with seven integration points (IP) across thickness have been selected to model the blank. The Gauss integration method, which is the numerical integration rule through the shell thickness, uses those integration points to capture the variation in physics throughout the shell thickness. Shell elements have been selected, rather than solid elements, because the nature of the SPIF process renders it possible to ignore the stress variation through the blank thickness, which is known as the state of "membrane stress". This will substantially help reducing the solving time. However, shell elements do not provide deformation history through the thickness[18]. Consequently, the determination of thinning is dependent on the Z-strain values. Since there are several options for shell elements, each with its own (KEYOPT), the Belytschko-Tsay model (ELFORM2) has been selected for this work as it is proved to be quite appropriate for the SPIF process.

V.3. NUMERICAL SIMULATION PRE-PROCESSING

Moreover, the material behaviour of the blank is defined using the (MAT_MODIFIED_PIECEWISE_LINEAR_PLASTICITY) card including the isotropic hardening curve, which has been previously obtained from the tensile test, as discussed above in section 2. The card includes the basic information required for any material such as density, young's modulus, Poisson's ratio, and yield stress. Besides, it also provides multiple methods to define the plasticity properties for the material, however, a load curve ID known as (LCSS) is employed to fit the card with the multilinear isotropic hardening curve.

A boundary condition has been defined so that the nodes near the edge of the blank are all constrained. That is because the blank in real situation is fixed all along the circumference. A set of nodes consisting of the rows of nodes following the edge of the blank is first defined as an individual set, separately from the other nodes at the rest of the blank. In addition, the (BOUNDARY_SPC_SET) card is employed to define the degrees of freedom for this set to be all zeros. The width of this set is decided based on the width of the strip of the blank under clamping, as discussed later in the following section.

Since the upper part of the tool plays no role in the forming process, it has been eliminated to reduce the size of the FE model. Therefore, the tool is modelled as a hemisphere of 10 mm diameter representing only the lower part of the tool that is in contact with the blank.The tool is assumed to be un-deformable, and thus, it has been defined as a rigid body. Being a rigid body, the material of the tool has been defined using the material card (MAT_RIGID), through which the FE-solver considers the elements as non-flexible with zero deformation allowed, whereas it can define the degrees of freedom through which the tool is only allowed to move. Moreover, a path has been assigned to the tool in terms of X, Y, and Z coordinates. The (PRESCRIBED_MOTION_RIGID) card has been used to define the displacement-vs.-time values for each of X, Y, and Z direction. The tool path has been defined based on the path previously generated by the CAM software, as discussed in section 3.

The contact between the tool and the blank has been defined using (FORMING_ONE_WAY_SURFACE_TO_SURFACE) card. This contact model is proved to realistically simulate the contact nature between bodies in forming processes in general. To define the contact, it should be first decided which of the bodies in contact is the slave and which is the master. The only rule is that the master should always be the rigid body, which is the tool in this case. Friction is neglected in this study as, in such experiments, lubricants are used extensively, and moreover, the tool's end is a hemisphere, so the contact area is relatively small. Besides, the contact settings are set so that the thickness change is considered in the contact formulation as long as the forming process works.

V.4. MESH INDEPENDENT TEST

Mesh independent test is commonly performed so as to make sure that the model is independent on any possible mesh variations. In other words, it is performed to guarantee that any change occurs in the results is only due to the change in the physics. In addition, the test also provides an optimum limit for the mesh size, beyond which, the FE model size is needlessly large. The test is carried out by changing the mesh size gradually from coarse to fine while observing the value of the resulted EPS until two successive values are similar within an accepted range (5%).

The mesh independent test is finally succeeded after four trials of changing the mesh size. As the mesh of the blank is divided into two regions -as previously mentioned- the mesh size is changed for both center and edge regions as 10, 20, 15, and 30 divisions for the center, and as 40, 80, 100, and 120 divisions for the edge. The EPS values of the last two trials are 2.713 and 2.825, which satisfies the 5% condition.

V.5. SPRINGBACK ANALYSIS

An important point that should be taken into consideration during the numerical simulation process is the springback, for it is natural for the blank to spring back after the impact of the tool is lifted. Taking that into consideration is of paramount importance when comparing the deformed profiles resulting from the simulation and the experiment. The card (INTERFACE_SPRINGBACK_LSDYNA) has been employed. This card is responsible for generating a file entitled (dynain), which contains the final profile generated from the simulation, and the history of stresses and strains as an initial condition[19].

A simple simulation is carried out using this file to find the value of springback, depending on the properties of the materials previously identified.

VI. RESULTS AND DISCUSSION

In this section, the results generated by the numerical

simulation are discussed together with a comparison to the results generated by the experiment.

Based on the forming parameters defined in section 3, the termination time has been set to 153 sec and 653 sec for the circular and rectangular taper pockets respectively. Finally, after finishing all the pre-processing, the keyword file has been generated and solved using LS-Dyna's solver. Figure 9 (a and b) show the results represented by the EPS distribution all over the blank for the circular and rectangular pockets respectively.

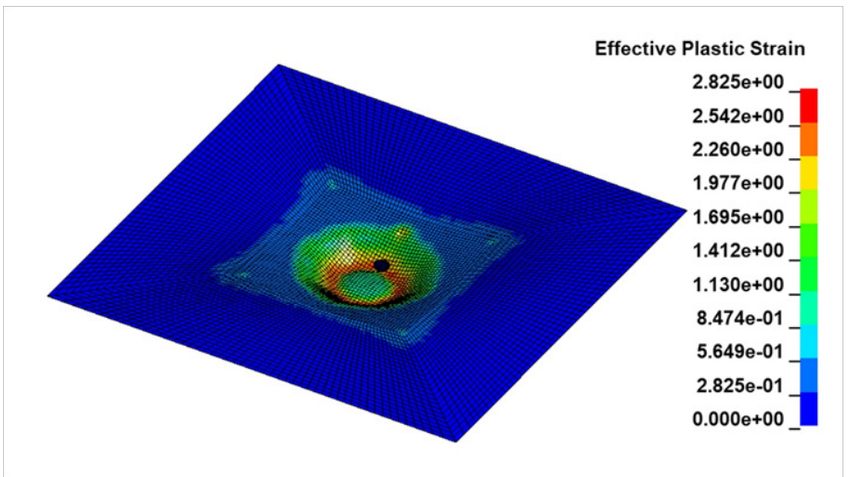

(a)

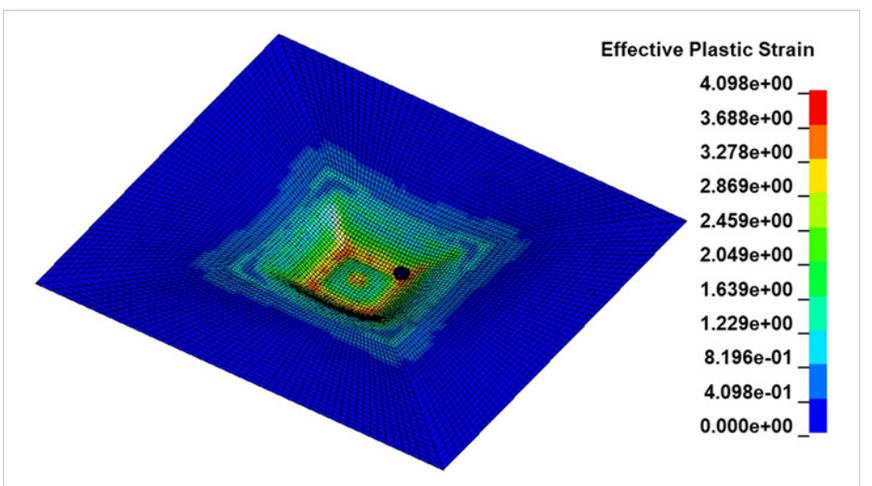

(b)

Fig. 9: The results of the simulation represented by the EPS distribution all over the blank for (a) circular and (b) rectangular taper pockets.

The graphs in Figure 10 (a and b) show for both the circular and rectangular taper pockets, the three cross-sectional profiles: the cross-sectional profile of the ideal design, the cross-sectional profile resulting from simulation, and the cross-sectional profile resulting from the experiment, all presented against one another. As shown in the graphs, the nodes at the edge of the blank show no contribution to the forming process since they are previously set to be fixed, whereas the maximum values of the Z-displacement are shown as a ring toward the middle of the blank. Three differences can be noted in these graphs: the pillow effect, the blank bending problem, and the springback. First, the area in the exact centre of the blank which has not been subjected directly to the tool throughout the process has not fully reached the desired depth, resulting in a concave shape known as the pillow effect. Secondly, the profiles resulting from the numerical simulation and the experiment are remarkably different

from the ideal design at the area which directly follows the fixation area, due to what is known as the blank bending problem. Finally, there is a difference between the desired depth of the ideal design and the depth that has actually been reached in both the simulation and experiment. This difference represents the springback.

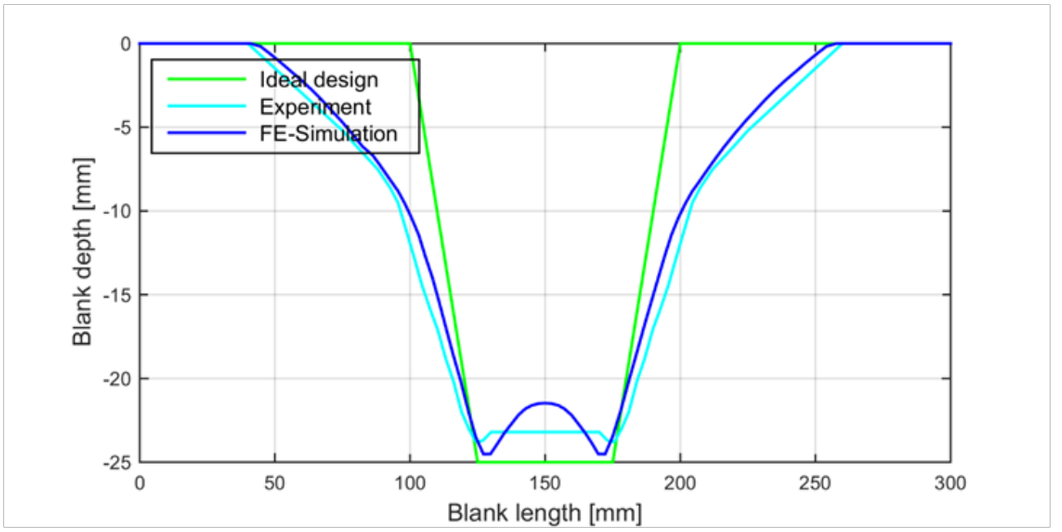

(a)

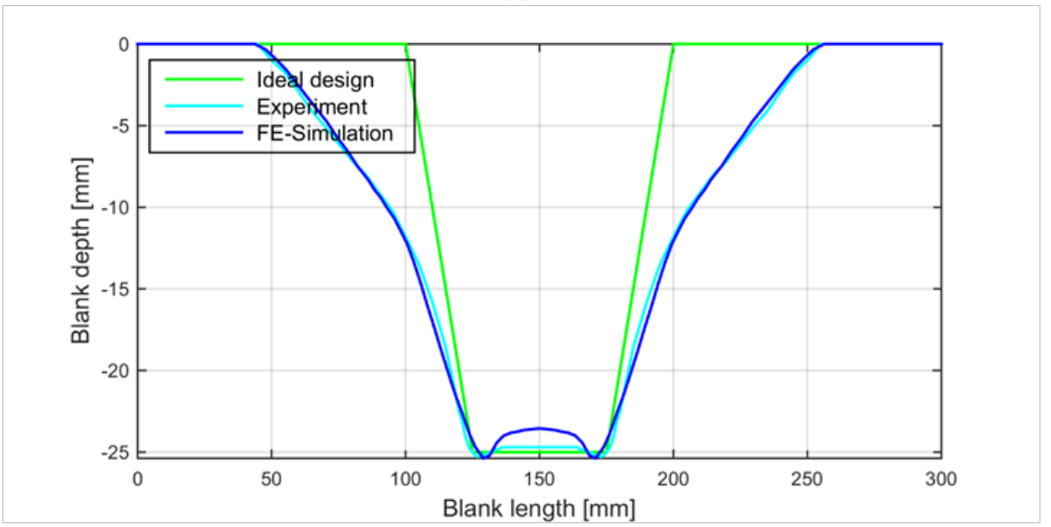

(b)

Fig. 10: the cross-sectional profile of the (a) circular and (b) rectangular pockets according to the ideal design, the simulation, and the experiment

Table 1 shows that the difference in the results of the thinning in the cases of the simulation and the experiment is minimal, where the difference does not exceed 8% in the circular shape and 10% in the rectangular shape. The same goes for the springback, where the difference in the circular shape is less than 6% and in the rectangular profile around 2.5%.

Table 1: Forming parameters and results obtained from numerical simulation and experiments for both circular and rectangular taper pockets.

	Circular profile		Rectangular profile	
	Sim.	Exp.	Sim.	Exp.
Incremental step size (δz) (mm)	0.5		0.2	
Feed rate (fr) (mm/min)	4000		6000	
Tool path length (m)	10.2		65.28	
Time(s)	153		653	
Thinning percentage (δt)	32.2	35	33.12	30
Spring back (mm)	1.13	1.2	1.23	1.2

Moreover, the force acting on the blank in Z-direction has been obtained throughout the time of the process for both circular and rectangular taper pockets, as shown in the graphs in Figure 11 (a and b). These graphs provide an estimation of the average force value, according to which the proper CNC machine for the process can be selected. This average has been found to be 6.94 KN for the circular shape and 4.22 KN for the rectangular one.

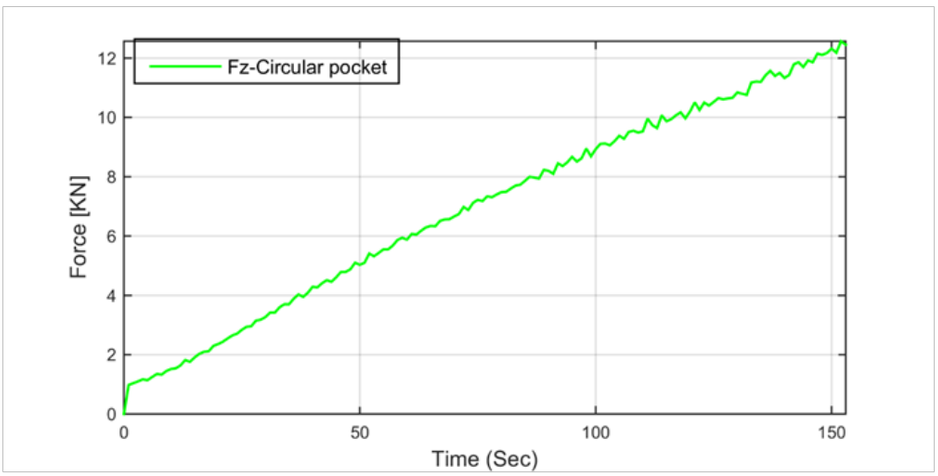

(a)

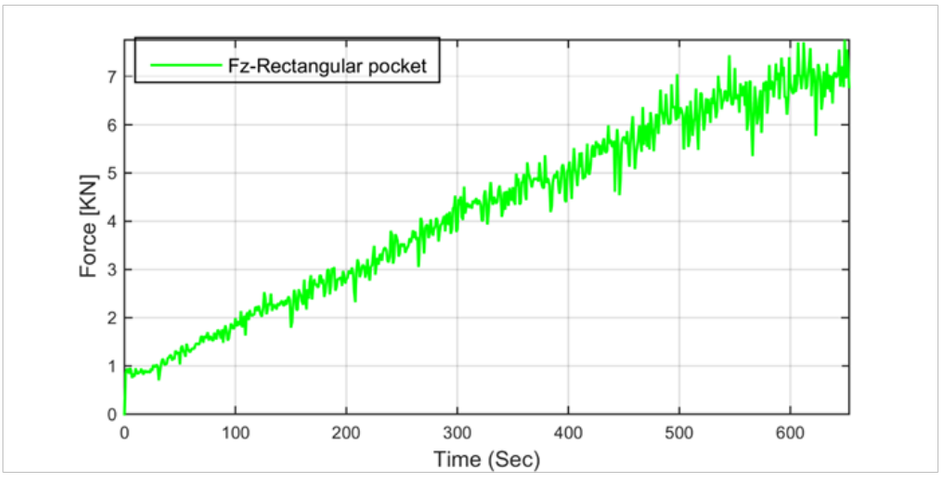

(b)

Fig. 11: The force acting on the blank in Z-direction throughout the time of the process for (a) circular and (b) rectangular taper pockets.

VII. CONCLUSION

This study has managed to present a realistic simulation of SPIF process. The simulation of SPIF process has been carried out using LS-Dyna4.3© software while producing a circular and rectangular taper pockets on a blank made of AL6061. The tool path has been generated using a CAM software based on the desired shapes, while the forming parameters such as the feed rate and the forming step has been defined. The SPIF process has been prepared to be executed on a CNC machine. The simulation has been validated to the experimental results in terms of thickness reduction, springback, and cross-sectional profile. The results of both simulation and experiment are proved to be close within an accepted range. The difference in the results of the thinning in the cases of the simulation and the experiment is minimal, where the difference does not exceed 8% in the circular shape and 10% in the rectangular shape. The same goes for the springback, where the difference in the circular shape is less than 6% and in the rectangular profile around 2.5%. In addition, as revealed in the numerical simulation, the average value of the force acting on the blank in Z-direction, obtained throughout the time of the process for both circular and rectangular taper pockets, has been found to be 6.94 KN for the circular shape and 4.22 KN for the rectangular one.

Any metal forming process usually includes more than a single design value or a single constraint, which renders obtaining the optimum parameters through an experiment a very costly process in terms of time and money. The simulation obtained in this study can be used in order to perform an optimization analysis to decide the optimum forming parameters that are thought to affect the SPIF process. Yet, since the numerical simulation of the SPIF has proved valid, it can be used to obtain the optimum design, and this is planned to be achieved in a future study.

VIII. REFERENCES

[1] Kopac, J., and Kampus, Z. Incremental sheet metal forming on CNC milling machine-tool. 13th international scientific conference on achievements in mechanical and materials engineering. 2005 ; pp. 335-338.

[2] Jeswiet, J., Micari, F., Hirt, G., Bramley, A., Duflou, J., and Allwood, J. Asymmetric single point incrmental forming of sheet metal. CIRP Annals - Manufacturing Technology. 2005; 54, pp. 623-650.

[3] Tisza, M. General overview of sheet incremental forming. Journal of Achievements in Materials and Manufacturing Engineering. 2012; 55(1), pp. 113-120.

[4] Nimbalkar, D. H., and Nandedkar, V. M. Review of incremental forming of sheet metal components. International Journal of Engineering Research and Application. 2013; 3(5), pp. 39-51.

[5] Hussain, G., Hayat, N., and Gao, L. An experimental study on the effect of thinning band on the sheet formability in negative incremental forming. International Journal of Machine Tools and Manufacture. 2008; 48, pp. 1170-1178.

[6] Hussein, G., and Gao, L. A novel method to test the thinning limits of sheet metals in negative incremental forming. International Journal of Machine Tools and Manufacture. 2007; 47, pp. 419-435.

[7] Naranjo, J. A., Miguel, V., Martínez, A., Coello, J., and Manjabacas, M. C. Evaluation of the formability and dimensional accuracy improvement of Ti6Al4V in warm SPIF processes. Metals. 2019; 9(3), 272.

[8] Afonso, D., de Sousa, R. A., and Torcato, R. Integration of design rules and process modelling within SPIF technology-a review on the industrial dissemination of single point incremental forming. The International Journal of Advanced Manufacturing Technology. 2018; 94(9-12), pp. 4387-4399.

[9] Eksteen, P. D., and Van der Merwe, A. F. Incremental sheet forming (ISF) in the manufacturing of titanium based plate implants in the biomedical sector. CIE42. 2012; pp. 131-1-131-7.

[10] Popp, M. MATEC Web. [Online]. Available from: https://www.matec-conferences.org/articles/matecconf/pdf/2019/39/matecconf_mse2019_04008.pdf [Accessed 2019].

[11] Suresh, K., Khan, A., and Regalla, S. P. Tool path definition for numerical simulation of single point incremental forming. Procedia Engineering. 2013; pp. 536-545.

[12] Al-Obaidi, B., and Hamdan, W. The effect study of parameters in (ISMF) on (surface roughness, time work and thickness distribution) for (AL-1060) sheet metal. International journal of Current Engineering and Technology. 2016; pp. 2277 – 4106.

[13] Hrairi, M., and Echrif, S. B. Process simulation and quality evaluation in incremental sheet forming. IIUM Engineering Journal. 2011; 12(3), 185-196.

[14] Sedaghat, H., Xu, W., and Zhang, L. Ultrasonic vibration-assisted metal forming: Consecutive modelling of acoustoplasticity and applications. Journal of Materials Processing Tech. 2019; 265, pp. 122-129.

[15] Suresh, K., and Regalla, S. P. Effect of mesh parameters in finite element simulation of single point incremental sheet forming process. Procedia materials science. 2014; 6, pp. 376-382.

[16] Azaouzi, M., and Lebaal, N. Tool path optimization for single point incremental sheet forming using response surface method. Simulation Modelling Practice and Theory. 2012; 24, 49-58.

[17] Maqbool, F., and Bambach, M. Dominant deformation mechanisms in single point incremental forming (SPIF) and their effect on geometrical accuracy. International Journal of Mechanical Sciences. 2018; 136, pp. 279-292.

[18] Essa, K. Finite element prediction of deformation mechanics in incremental forming processes . University of Birmingham. 2011;

[19] Maker, B. N., and Zhu, X. Input parameters for springback simulation using LS-DYNA. 2001